NEOPLASIA
www.neoplasia.com

Volume 12 Number 11 November 2010 pp. 915–927 915

Stromal Activation Associated with Development of Prostate Cancer in Prostate-Targeted Fibroblast Growth Factor 8b Transgenic Mice[1,2]

Teresa D. Elo*, Eeva M. Valve*,†, Jani A. Seppänen*,‡, Heikki J. Vuorikoski*,‡, Sari I. Mäkelä*,§, Matti Poutanen¶,#, Paula M. Kujala and Pirkko L. Härkönen*,††**

*Department of Cell Biology and Anatomy, Institute of Biomedicine, University of Turku, Turku, Finland; †Department of Pharmacology, Drug Development and Therapeutics, University of Turku, Turku, Finland; ‡Pharmatest Services Ltd, Turku, Finland; §Functional Foods Forum and Department of Biochemistry and Food Chemistry, University of Turku, Turku, Finland; ¶Department of Physiology, Institute of Biomedicine, University of Turku, Turku, Finland; #Turku Center for Disease Modeling, University of Turku, Turku, Finland; **Department of Pathology, Tampere University Hospital, Tampere, Finland; ††Department of Laboratory Medicine, MAS University Hospital, Lund University, Lund, Sweden

Abstract

Expression of fibroblast growth factor 8 (FGF-8) is commonly increased in prostate cancer. Experimental studies have provided evidence that it plays a role in prostate tumorigenesis and tumor progression. To study how increased FGF-8 affects the prostate, we generated and analyzed transgenic (TG) mice expressing FGF-8b under the probasin promoter that targets expression to prostate epithelium. Prostates of the TG mice showed an increased size and changes in stromal and epithelial morphology progressing from atypia and prostatic intraepithelial neoplasia (mouse PIN, mPIN) lesions to tumors with highly variable phenotype bearing features of adenocarcinoma, carcinosarcoma, and sarcoma. The development of mPIN lesions was preceded by formation of activated stroma containing increased proportion of fibroblastic cells, rich vasculature, and inflammation. The association between advancing stromal and epithelial alterations was statistically significant. Microarray analysis and validation with quantitative polymerase chain reaction revealed that expression of osteopontin and connective tissue growth factor was markedly upregulated in TG mouse prostates compared with wild type prostates. Androgen receptor staining was decreased in transformed epithelium and in hypercellular stroma but strongly increased in the sarcoma-like lesions. In conclusion, our data demonstrate that disruption of FGF signaling pathways by increased epithelial production of FGF-8b leads to strongly activated and atypical stroma, which precedes development of mPIN lesions and prostate cancer with mixed features of adenocarcinoma and sarcoma in the prostates of TG mice. The results suggest that increased FGF-8 in human prostate may also contribute to prostate tumorigenesis by stromal activation.

Neoplasia (2010) 12, 915–927

Abbreviations: AP, anterior prostate; AR, androgen receptor; CTGF, connective tissue growth factor; DLP, dorsolateral prostate; FGF-8, fibroblast growth factor 8; FGFR, fibroblast growth factor receptor; mPIN, mouse prostatic intraepithelial neoplasia; SPP1, osteopontin; TG, transgenic; VP, ventral prostate; WT, wild type

Address all correspondence to: Teresa D. Elo, MSc, PhD Student, Department of Cell Biology and Anatomy, Institute of Biomedicine, University of Turku, Kiinamyllynkatu 10, FIN-20520 Turku, Finland. E-mail: tedoel@utu.fi

[1]This work was supported by grants from the Finnish Cancer Foundation, the Sigrid Jusélius Foundation, the Finnish Cultural Foundation and Turku University Foundation.
[2]This article refers to supplementary materials, which are designated by Tables W1 and W2 and Figures W1 and W2 and are available online at www.neoplasia.com.
Received 2 June 2010; Revised 16 July 2010; Accepted 19 July 2010

DOI 10.1593/neo.10776

Introduction

Fibroblast growth factors (FGFs) are polypeptide growth factors involved in various normal and pathologic processes. Their effects are mediated by FGF receptors (FGFRs), which are transmembrane tyrosine kinase receptors expressed as various splice variants with differential ligand binding specificities [1]. In prostate, FGFs and their receptors regulate embryonic development and maintain tissue homeostasis in the adult by means of directional signaling and reciprocal interactions between the epithelial and stromal compartments [2]. Elevated levels of various FGF ligands as well as aberrant expression of FGFRs have been reported in human prostate cancer and metastases [2,3], and disruption of FGF pathways in genetically engineered mouse models has provided evidence for the involvement of aberrant FGF signaling in prostate tumorigenesis [4–8].

Fibroblast growth factor 8 (FGF-8) is one of the FGF family members associated with prostate cancer [9–12] as well as breast [13] and ovarian cancer [14]. FGF-8 is a mitogenic and transforming growth factor that has important and widespread roles in embryonic development but a strictly restricted expression pattern in adult tissues [15]. It is expressed and secreted by the epithelium, and it signals directionally to mesenchyme by binding FGFR3c, FGFR4, FGFR2c, or FGFR1c [16,17]. There are four isoforms (a, b, e, and f) of human FGF-8 [18], of which the b-isoform has been shown to have the strongest transforming potential *in vitro* [19].

Several studies have shown up-regulation of FGF-8 expression in prostate cancer [9–11], and FGF-8 level has been reported to correlate with advanced stage and high grade of tumors [12,20] as well as with decreased patient survival [21]. We reported previously that FGF-8 is elevated in human premalignant PIN lesions [11], suggesting that this factor is involved in the early steps of prostate tumorigenesis. This conclusion was supported by the study of Song et al. [4] who demonstrated that prostate-targeted expression of *FGF-8b* induces development of mouse prostatic intraepithelial neoplasia (mPIN) lesions in transgenic (TG) mice. Besides tumorigenesis, our previous *in vitro* and *in vivo* studies have shown that FGF-8 is also involved in later stages of tumor progression by increasing tumor cell invasion and migration as well as angiogenesis and bone metastasis [22–25].

To study the mechanisms by which increased FGF-8 affects the prostate, we generated a TG mouse model expressing *FGF-8b* in prostate epithelium under the probasin (ARR_2PB) promoter [26] in the genetic background of the FVB/N strain. Our data show that mPIN lesions were frequently observed in TG mice older than 10 months as reported in the corresponding mouse model of Song et al. [4] generated in the C57BL/6 × DBA2 strain. Our study also demonstrates that, in addition to mPIN lesions, some old TG individuals developed prostate cancer with heterogeneous histology, sharing characteristics of both adenocarcinoma and sarcoma. Importantly, strong activation of prostate stroma was seen in young 3- to 6-month-old TG mice before and in association with mPIN formation. Our microarray analyses of the genes differentially expressed in the TG mouse prostates demonstrated that genes for connective tissue growth factor (*CTGF*) and osteopontin (*SPP1*) were upregulated in TG mouse prostates. There were also marked changes in expression of epithelial and stromal androgen receptor (AR). The results underline the capacity of FGF-8b to induce prostate cancer and the importance of stromal activation in FGF-8b–induced prostate tumorigenesis and tumor progression.

Materials and Methods

Generation of ARR_2PB–FGF-8b Transgenic Mouse Lines

A 530-bp-long DNA fragment containing the probasin (ARR_2PB) promoter was digested from pBluescipt II SK+ vector and ligated to a pcDNA 3.1(–) expression vector in front of human FGF-8b complementary DNA (cDNA). A 1.8-kb-long DNA fragment containing the transgene construct (Figure 1*A*) was then excised from the pcDNA 3.1(–) vector using *Xho*I and *Dra*III and ligated to the promotorless pGEM7Zf(+) vector for functional testing *in vitro*. Transgene construct was purified from agarose gel by using a Quick-Pick electroelution Capsule kit (Qiagen, Valencia, CA) and Elutip DEAE columns (Schlaicher & Shüell, Dassel, Germany) and thereafter microinjected into the pronuclei of fertilized FVB/N mice oocytes.

Total DNA was extracted from tail or ear biopsies of the offspring, using DNeasy columns (Qiagen), and the presence of the transgene was tested by using genotyping polymerase chain reaction (PCR; Figure W1*A*) with primers 5′-TACAACTGCCAACTG GGATG-3′ (forward) and 5′-GGCGGGTAGTTGAGGAACTC-3′ (reverse) specific for the transgene construct. Mice positive for the transgene were used as founder mice and mated with WT FVB/N mice to establish four

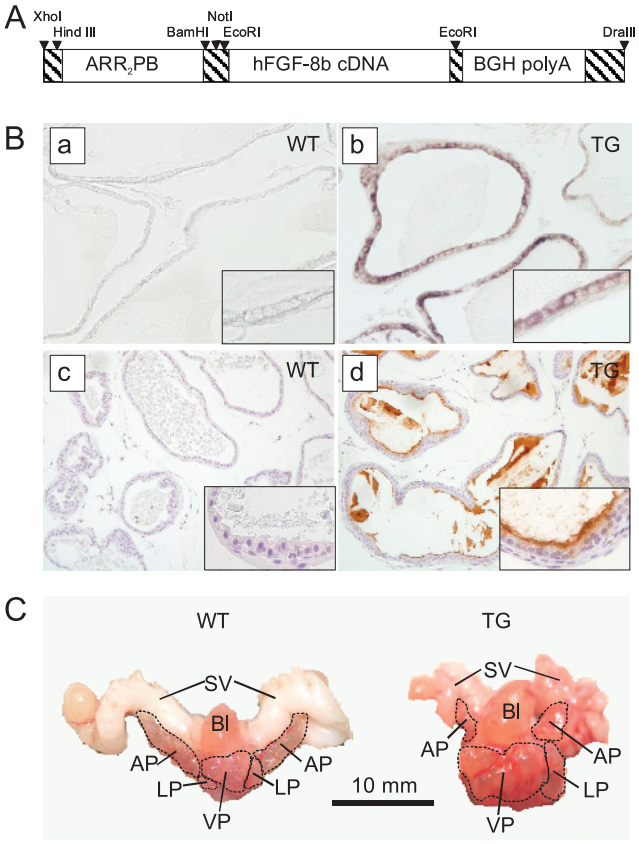

Figure 1. Generation and characterization of FGF-8b transgenic mice. (A) The transgene construct. (B) Transgene expression was localized to VP of TG mice by *in situ* hybridization with FGF-8b–specific riboprobes (a, b) and by FGF-8b immunostaining (c, d). Expression of FGF-8b was absent or low in VP samples of WT mice. (C) Representative pictures of prostate blocks from a 13.5-month-old WT and a 14-month-old FGF-8b TG mouse showing the abnormal, cystic appearance of TG mouse prostate. Bl indicates bladder; LP, lateral prostate; SV, seminal vesicle.

FGF-8b TG mouse lines (nominated as L2-L5) used for further analysis of the transgene expression and phenotypic features. Animal studies were approved by the Finnish Animal Ethics committee, and the institutional policy on animal experimentation fully meets the requirements as defined in the National Institutes of Health's guide on animal experimentation.

Tissue Preparation

After killing the mice, their body weights were measured, and tissues of interest for RNA extraction were quickly prepared and frozen in liquid nitrogen. For histologic preparations, prostate blocks or prostate lobes were removed, weighed, and fixed overnight in 10% neutral-buffered formalin. Fixed tissues were embedded in paraffin, and 5-μm sections for standard hematoxylin and eosin staining, immunohistochemistry (IHC), and *in situ* hybridization were prepared.

Androgen Treatment of Prepubertal Mice

For this study, 14-day-old TG (n = 13) and WT (n = 7) male mice were treated for a 2-week period with subcutaneous daily injections of testosterone propionate (7 μg/g of body weight; Sigma-Aldrich Chemie GmbH, Steinheim, Germany) dissolved in maize oil (+1% ethanol). Control animals were treated with corresponding amounts of the solvent.

RNA Extraction and Reverse Transcription–PCRs

Total RNA from tissues was extracted using TRIzol reagent according to the manufacturer's instructions (Invitrogen, Life Technologies, Inc, Carlsbad, CA). After isolation, the RNA was purified and treated with DNAse in RNeasy columns (Qiagen).

In reverse transcription–PCRs (RT-PCRs), 1 μg of total RNA was used for cDNA synthesis as described earlier [27]. The sequences of the primers used in FGF-8b–transgene–specific RT-PCR were 5′-GGACACCTTTGGAAGCAGAG-3′ (forward) and 5′-CAACAGATGGCTGGCAACTA-3′ (reverse) and those in β-actin RT-PCR were 5′-TTGTAACCAACTG GGACGATATGG-3′ (forward) and R 5′-GATCTTGATCTTCATGGTGCTAGG-3′ (reverse).

In quantitative RT-PCRs (qRT-PCRs), cDNA were amplified using Quantitect SYBR green reagent (Qiagen) for two-step RT-PCR with amplification conditions recommended by the manufacturer's handbook. Reactions were performed in triplicate in DNA Engine Opticon (MJ Research, Inc, Waltham, MA). Primer sequences for FGF-8b qRT-PCR were 5′-CCAAGCCCAGGTAACTGTTCA-3′ (forward) and 5′-AGGACCTGCACGTGCTTC-3′ (reverse) and those for β-actin qRT-PCR were 5′-CGTGGGCCGCCCTAGGCACCA-3′ (forward) and 5′-TGGCCTTAGGGTTCAGGGGG-3′ (reverse). Relative expression levels were calculated by the $2^{-\Delta\Delta CT}$ method [28] using *β-actin* as a reference gene.

FGF-8b In Situ Hybridization

Human FGF-8b cDNA derived from pcDNA 3.1 (–) expression vector was used as a template in a PCR to amplify the FGF-8b sequence for riboprobe synthesis. Sequences of the PCR primers used containing the binding sites of T7 and T3 RNA polymerases (indicated with bold letters) were 5′-CAGAGATGCA**TAATACGACTCACTATAGGGAGA**CCAA GCCCAGGTAACTGTTCAGTCC-3′ (forward) and 5′-CCAAGCCTTC**ATTAACCCTCACTAAAGGGAGA**-TTCCCCTTCTTGTTCATGCAGATGT-3′ (reverse). Purification of the PCR product and synthesis of the digoxigenin-labeled riboprobes, as well as pretreatment of sample slides, the hybridization procedure, and the subsequent treatments were carried out as described previously [29]. Hybridization was performed overnight at 55°C with probe concentrations of 100 ng/ml.

Histologic Classification

Histologic analysis of prostates (n = 72 TG mice from lines L2, L4, and L5 and n = 43 littermate WT mice) using the Bar Harbor classification system [30] was performed in a blinded manner (T.E.). The results of the analysis were confirmed by a clinical pathologist (P.K.).

Immunohistochemical Stainings

Paraffin-embedded sections were used for immunostaining, with the exception of CD68 staining, which was performed using frozen sections. Antigen retrieval was performed with 10 mM citrate buffer, pH 6, in a microwave oven (FGF-8b, CD3, and CD45R/B220 stainings), with citric acid buffer, pH 6, in a pressure cooker (AR staining), with proteinase K (cytokeratin staining) or Ficin (Zymed, San Francisco, CA) at 37°C (laminin staining). Antibodies used were anti–FGF-8b (AF-423-NA; R&D Systems, Abingdon, UK), anti-AR (SC-816; Santa Cruz Biotechnology, Santa Cruz, CA), anti-CD3 (ab5690; Abcam, Cambridge, UK), anti-CD45R/B220 (550286; BD Pharmingen, San Diego, CA), anti-CD68 (MCA1957; AbD Serotec, Kidlington, UK), anti-SMA (MS-113-P; NeoMarkers, Fremont, CA), antilaminin (L9393; Sigma-Aldrich, St Louis, MO), anticytokeratins (Z0622; DAKO, Glostrup, Denmark), and anti-SPP1 (AF808; R&D Systems). Biotinylated secondary antibodies, avidin-biotinylated peroxidase complex (Vectastain ABC kit, PK-4000; Vector, Inc, Burlingame,

Table 1. Genes Analyzed and Primers Used in the Probe Library qRT-PCR.

Gene (Symbol)	Primers 5′-3′
Apolipoprotein D (*APOD*)	F: ACGGAAACATCGAAGTGCTAA, R: TGGCTTCACCTTTACTTGG
Clusterin (*CLU*)	F: TGCTGATCTGGGACAATGG, R: CTCCCTTGAGTGGACAGTTCTT
Connective tissue growth factor (*CTGF*)	F: TGACCTGGAGGAAAACATTAAGA, R: AGCCCTGTATGTCTTCACACTG
Early growth response (*EGR1*)	F: CCTATGAGCACCTGACCACA, R: TCGTTTGGCTGGGATAACTC
Forkhead box Q1 (*FOXQ1*)	F: CAGGTCGGTGCCTGAGAC, R: CGCTTATGCTATCGGTCTGG
Lipocalin (*LCN2*)	F: CCATCTATGAGCTACAAGAGAACAAT, R: TCTGATCCAGTAGCGACAGC
Ribosomal protein L19 (*L19*)	F: TCGTTGCCGGAAAAACAC, R: CCGAGCATTGGCAGTACC
Secreted phosphoprotein, osteopontin (*SPP1*, *OPN*)	F: CCCGGTGAAAGTGACTGATT, R: TTCTTCAGAGGACACAGCATTC
Seminal vesicle protein secretion 2 (*SVS2*)	F: ACAGTCAGCTGTGTTTGTACAATATG, R: GCCTTTCTGACCAAGCATAAA
Small proline-rich protein 1A (*SPRR1A*)	F: CCTGAAGACCTGATCACCAGA, R: AGGCAATGGGACTCATAAGC
Small proline-rich protein 2A (*SPRR2A*)	F: CTGCTCCGGAGAACCTGAT, R: ACAAGGCTCAGGGCACTTC
Sonic hedgehog (*SHH*)	F: TCCACTGTTCTGTGAAAGCAG, R: GGGACGTAAGTCCTTCACCA
Transglutaminase 4 (*TGM4*, *EAPA1*)	F: TGCAGAGAGAGGTAGCAGGAC, R: TCTCTCCACATTCACAGCGTA
Unknown gene (GI 38086179)	F: CCTGGAGGACAGACAGCATC, R: TGGCAGGAATGTGTACAGATAGA

CA) and 3,3′-diaminobenzidine (DAB substrate kit SK-4100; Vector, Inc) were used for visualization, and Mayer hematoxylin was used for counterstaining.

Microarray Analysis

Illumina Sentrix Mouse-6 oligomicroarray BeadChips (Illumina, San Diego, CA) containing 47,769 oligos were used for studying gene expression levels in the ventral prostates (VPs) of 3-month-old TG and WT mice ($n = 3$ per group). Quality control of RNA and the microarray hybridization protocol were performed at the Finnish DNA microarray center (Turku, Finland) according to the manufacturer's protocol.

Gene Spring 7.2 software (Agilent Technologies, Santa Clara, CA) was used for analysis of the microarray data and Ingenuity Pathways analysis software (IPA, Ingenuity Systems; http://www.ingenuity.com) for mining the data and constructing functional regulatory networks. Microarray data verification concerning 13 selected genes (Table 1) in the VPs of 3-month-old TG and WT mice ($n = 5$ per group) was carried out by means of a probe-based qRT-PCR method (ProbeLibrary; Roche Diagnostics GmbH, Roche Applied Science, Basel, Switzerland) at the Turku Center of Biotechnology. An online assay design program (Probe Finder; http://www.universalprobelibrary.com) was used to design suitable primer pairs (Table 1). *L19* was used as a housekeeping gene for normalization of the expression levels. The expression of SPP1 and CTGF were further studied, using the same primers, by means of the SYBR green–based qRT-PCR method as described earlier.

Scoring the Histologic Changes and Immunohistochemical Stainings

For statistical analysis studying the association between the epithelial and stromal changes and between the epithelial changes and inflammation, TG mice (aged 9-20 months, $n = 49$) were divided into four groups according to the most advanced histologic change in their prostate epithelium (normal, hypercellular, mPIN, and carcinoma). Age of mice did not differ between the groups (analysis of variance, $P = .093$). A numeric score (from 1 to 4) was given to each sample according to the most advanced histologic change present in the prostate stroma as follows: 1, normal stroma; 2, hypercellular stroma; 3, atypical stroma; and 4, malignant stroma. Evaluation of the degree of prostatic inflammation (scores from 0 to 3) was based on the mean number of inflammatory cell aggregates in the prostate stroma in ×40 microscopic field as follows: 0, no signs of inflammation; 1, mild inflammation presented by one to three aggregates of inflammatory cells; 2, moderate inflammation with four to seven aggregates of inflammatory cells; and 3, pronounced inflammation with more than seven large aggregates of inflammatory cells.

Staining grade of AR was defined from sections stained by AR IHC by estimating the percentage of positively stained nuclei in the VP epithelium and stroma (WT, $n = 9$, aged 3-16 months; TG, $n = 13$, aged 3-18.5 months). In cases of normal histology or stromal proliferation, the mean percentage of AR-positive cells was defined by evaluating at least five representative microscopic fields at ×400 magnification. For mPIN lesions, the proportion of AR-positive cells was estimated for each mPIN containing acinus, and the mean proportion per acinus was calculated. For carcinoma, stromal atypia, and sarcoma, total areas containing the respective changes were evaluated.

Statistical Analysis

Statistical analyses were carried out using SPSS 11.0 for Windows (SPSS, Inc, Chicago, IL). The normality of distributions was tested by using the Shapiro-Wilk W test. Differences between groups were thereafter tested by the two-sample t-test, the Mann-Whitney U test, or the analysis of variance. In analysis containing multiple comparisons, Bonferroni corrections for P values were applied. Logistic regression analyses (LRAs) were applied to study which histologic changes (inserted as binary categorical variables: present or absent) could predict the presence of mPIN lesions in TG mouse prostates. The predictive ability of each factor was studied separately and adjusted for age. Values of $P < .05$ were considered statistically significant.

Results

Generation and Analysis of FGF-8b Transgenic Mice

Four FGF-8b TG mouse lines (L2-L5) were generated, and their analysis by RT-PCR showed that *FGF-8b* was expressed in the ventral, dorsolateral, and anterior prostate (VP, DLP, and AP), the ductus deferens, the urethra, the epididymides, and the seminal vesicles of 3-month-old TG animals with the highest expression in VP (Figure W1*B*). No significant expression was detected in other tissues studied. According to the qRT-PCR data, *FGF-8b* messenger RNA (mRNA) levels in the VPs of all four TG mouse lines were hundred to several thousand times higher than in the WT mice, and the expression levels remained high in the VPs of old (12- to 16-month-old) TG mice (Figure W1*C*). By way of *in situ* hybridization and FGF-8 IHC, transgene expression was detected in prostate epithelia (Figure 1*B*) of young and old TG mice. In line with the qPCR data, the staining was strongest in the VP.

Figure 2. FGF-8b transgenic mice develop advancing histologic changes in prostate epithelium and stroma. (A) Representative pictures of histologic changes in hematoxylin and eosin–stained sections (a, WT; b-i, TG). Normal VP histology, WT, 16-month-old (a); stromal hypercellularity and increased vasculature in VP, TG, 4-month-old (b); hypercellularity of VP epithelium, TG, 6-month-old (c); mucinous metaplasia in VP, TG, 13-month-old (d); advanced mPIN lesion in VP, TG, 16-month-old (e); adenocarcinoma in VP, TG, 13-month-old (f); atypical stromal hypercellularity showing phyllodes growth pattern and inflammation, TG, 14.5-month-old (g); sarcoma in VP, TG, 13-month-old (h); and carcinosarcoma in VP, TG, 18.5-month-old (i). Images were taken at ×100 to ×200 magnification, and inserts were taken at ×400 magnification. Scale bars, 100 μm. (B) Frequencies (%) of histologic changes in the oldest age group (12-21 months old) of TG and WT mice. Carcinosarcomas were included in the sarcoma group. (C) Immunohistochemical staining of FGF-8b in neoplastic lesions of FGF-8b TG mouse prostates. VP glands with normal-appearing histology located next to a big carcinosarcoma lesion in a TG prostate (a), mPIN lesions in the VP of a TG mouse (b), adenocarcinoma in the VP of a TG mouse (c), and carcinosarcoma in the same prostate as the normal-appearing glands in subpanel a (d). Images were taken at ×200 magnification. Scale bars, 100 μm. (D) Association between epithelial and stromal changes in TG prostates. Mean scores of stromal phenotypes in TG mouse groups (9-20 months old) defined by the histologic status of prostatic epithelium. Numeric values (1-4) for stromal phenotype were given as indicated in the Materials and Methods section. The bars show the means ± SEs. Statistical significance was assessed with the Mann-Whitney U tests, and Bonferroni corrections were applied. ***$P < .001$, *$P < .05$.

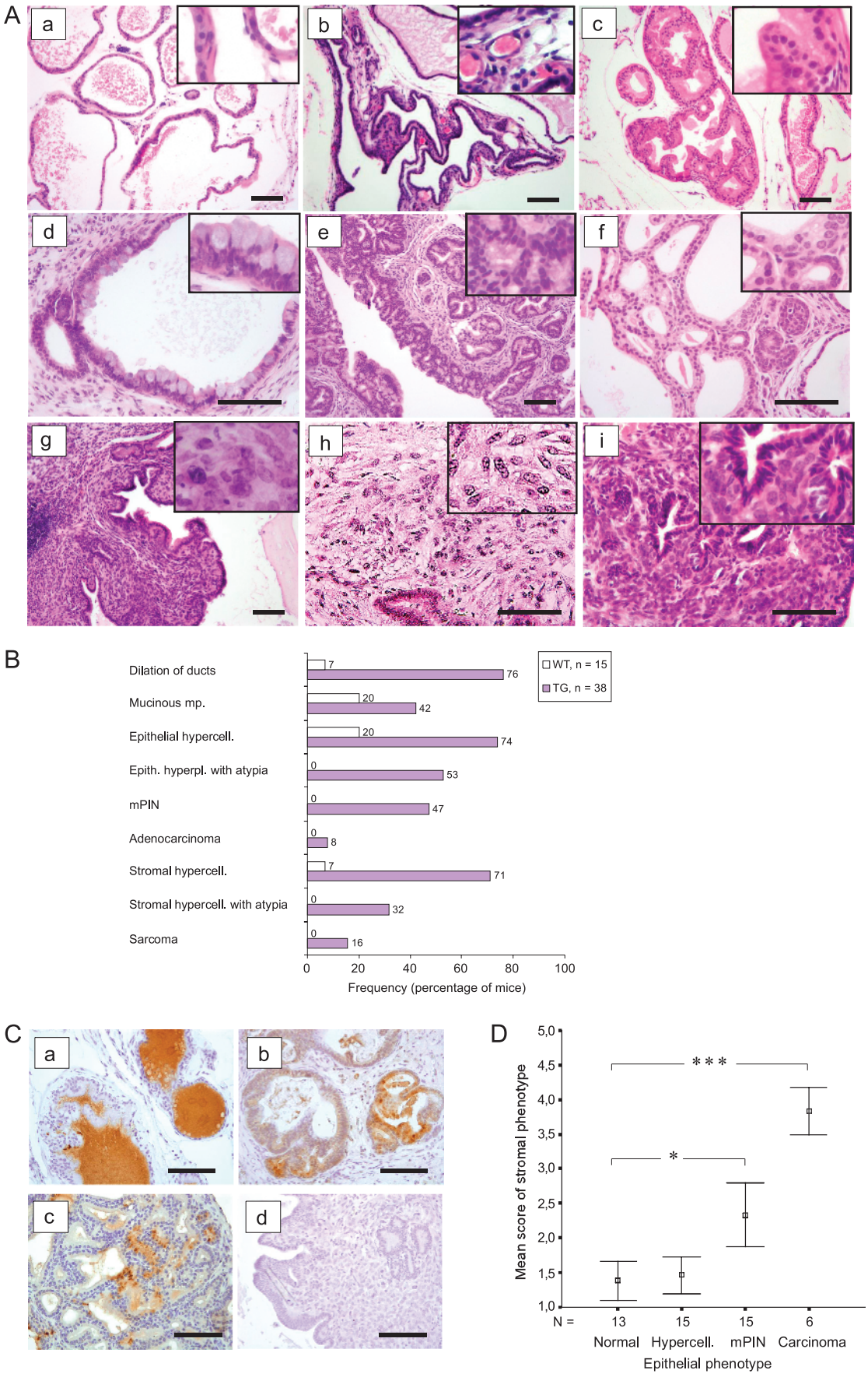
A
a
b
c
d
e
f
g
h
i
B
Dilation of ducts
Mucinous mp.
Epithelial hypercell.
Epith. hyperpl. with atypia
mPIN
Adenocarcinoma
Stromal hypercell.
Stromal hypercell. with atypia
Sarcoma
7
76
20
42
20
74
0
53
0
47
0
8
7
71
0
32
0
16
WT, n = 15
TG, n = 38
0
20
40
60
80
100
Frequency (percentage of mice)
C
a
b
c
d
D
Mean score of stromal phenotype
5,0
4,5
4,0
3,5
3,0
2,5
2,0
1,5
1,0
* * *
*
N =
13
15
15
6
Normal
Hypercell.
mPIN
Carcinoma
Epithelial phenotype

Epithelial Overexpression of FGF-8b Induces Morphologic Changes in the Prostate and Other Urogenital Organs

Altogether, 133 TG mice at ages varying from 2.5 to 20 months were macroscopically examined and compared with WT littermates at autopsy. The gross phenotype or body weights of the TG animals did not differ from those of their WT littermates (data not shown). The weights of the VP and the DLP were higher in TG mice, the difference being statistically significant in mice older than 6 months (VP) and 8 months (DLP), respectively (Figure W2). The VPs of TG mice were not only increased in size but also presented swellings, hemorrhagic cysts, and tumors, especially in TG mice older than 10 months.

In some TG animals, morphologic changes, such as increased size, swellings, or tumor-like morphology, were also observed in epididymides and seminal vesicles (data not shown). Accordingly, male infertility with a varying frequency (33%-75%) was observed in three TG mouse lines. Studies on the mechanisms underlying the infertility/subfertility are ongoing.

FGF-8b TG Mice Develop Stromal Hypercellularity, mPIN, and Neoplastic Lesions with Mixed Histology of Adenocarcinoma and Sarcoma

Histologic analysis of TG mice (L2, L4, and L5) revealed progressive changes in prostate epithelium and stroma, with frequencies and severity increasing on aging (Figure 2, *A* and *B*, and Table W1). Most changes (75%) were located in the VP, whereas some were also found in DLP and less frequently in AP.

The most obvious change in the VPs of young (3- to 6-month-old) TG mice compared with WT mice was the mild or moderate stromal hypercellularity (frequency, 56%) often associated with increased vasculature (Figure 2*A*, *b*). VPs of young TG mice also frequently contained epithelial changes such as hypercellularity, dilation of acini, and mucinous metaplasia (Figure 2*A*, *c* and *d*). Epithelial hyperplasia with atypia characterized by cells with enlarged hyperchromatic nuclei became more common in older (>6-month-old) TG mice. Focal or multifocal mPIN lesions (Figure 2*A*, *e*) were first observed in 7- to 11-month-old TG mice (19%) and in almost half (47%) of the older TG mice (>12-month-old). Besides mPIN lesions, malignant changes classified as adenocarcinoma (Figure 2*A*, *f*) were found in VPs of some old TG individuals (8%). Atypical changes in the stroma, characterized by big abnormal cells (Figure 2*A*, *g*), with enlarged nuclei and numerous prominent nucleoli, were first observed in 10-month-old TG mice and became more common in mice older than 12 months (32%). In some cases, the expanded atypical stroma presented a focal phyllodes-type growth pattern (Figure 2*A*, *g*). On the basis of the destructive growth pattern, prominent mitotic activity, markedly increased cellularity, and marked nuclear atypia, stromal atypias were classified as sarcomas (Figure 2*A*, *h* and *i*) in six animals. In five of these, both adenocarcinoma and sarcoma-like tumor areas were found in the same prostate, and in three of these, the lesions were classified as carcinosarcomas because the adenocarcinoma and sarcoma-like areas colocalized (Figure 2*A*, *i*).

Expression of FGF-8b in the neoplastic lesions was studied by FGF-8b immunostaining (Figure 2*C*). In all the prostates with neoplastic lesions, the glandular epithelium with normal-appearing histology showed positive staining for FGF-8b in the epithelial cell cytoplasm and/or in the luminal secretion (Figure 2*C*, *a*). Most mPIN lesions showed FGF-8b immunoreactivity at least in some places (Figure 2*C*, *b*). Most tumor cells in adenocarcinoma lesions also stained positively for FGF-8b (Figure 2*C*, *c*). Sarcomatous areas did not show any staining, and tumor cells in carcinosarcoma were not stained either (Figure 2*C*, *d*).

mPIN Lesions and Malignant Changes in FGF-8b TG Prostates Are Associated with Stromal Changes and Inflammation

Stromal and epithelial changes and aberrances often coexisted in the same prostates. The mean score of stromal phenotype, increasing with

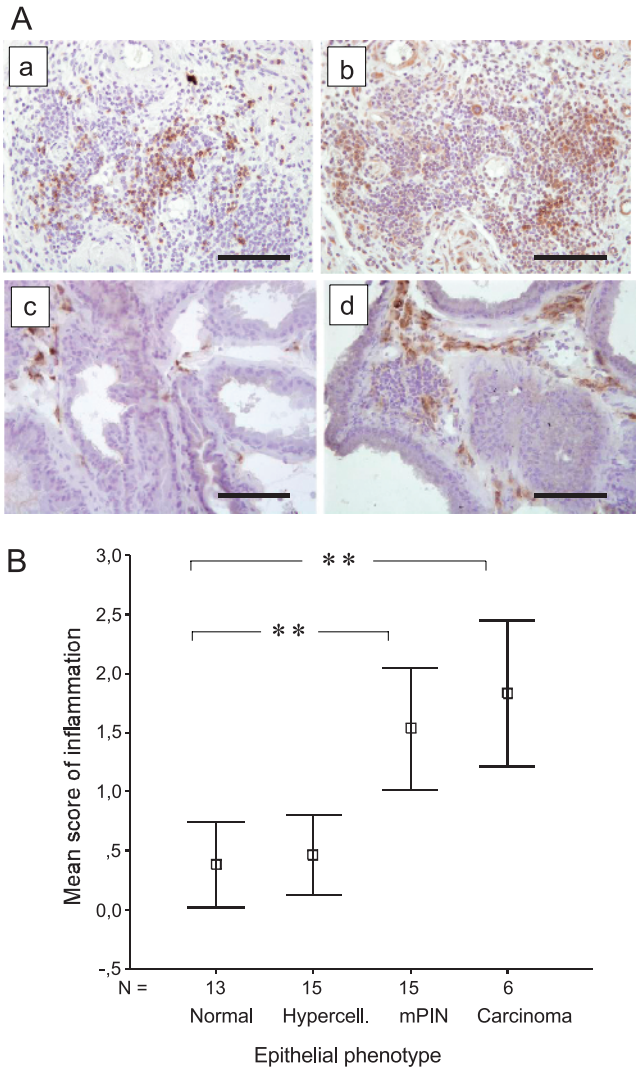

Figure 3. Aggregates of inflammatory cells in TG prostates are associated with epithelial changes. (A) Detection of inflammatory cell types by IHC staining. B-cell–specific CD45R IHC in a TG VP presenting pronounced inflammation in the prostatic stroma (a). T-cell–specific CD3 IHC in the same region as in subpanel a (b). Macrophage-specific CD68 IHC staining in WT mouse VP (c) and in TG mouse VP (d). Magnification, ×200. Scale bars, 100 μm. (B) Degree of inflammation in TG mouse groups (9-20 months old) defined by the histologic status of prostatic epithelium (groups as in Figure 2*C*). Evaluation and scoring (scores 0-3); the degree of inflammation was performed as described in the Materials and Methods section. The bars show the means ± SEs. Statistical significance was assessed with the Mann-Whitney *U* tests, and Bonferroni corrections were applied. $^{**}P < .01$, $^{*}P < .05$.

the severity of stromal changes, was found to be significantly higher (Mann-Whitney *U* test) in TG prostates containing mPIN lesions or adenocarcinoma compared with TG prostates with normal epithelium (Figure 2*D*).

Inflammation was also a common finding (incidence, >50%) in prostates of 7- to 21-month-old TG mice (Table W1). Immunohistochemical stainings for the expression of CD3, CD45R/B220, and CD-68 demonstrated that the aggregates of inflammatory cells contained T cells, B cells, and numerous macrophages (Figure 3*A*). Aggregates of inflammatory cells were often found in the prostatic stroma adjacent to mPIN lesions usually scattered in the prostatic stroma (Figures 2*A*, *b* and *g*, and 3*A*), but in some cases of pronounced inflammation (score 2-3), they were also found in the glandular lumina. The degree of inflammation was found to be significantly higher (Mann-Whitney *U* test) in TG prostates containing mPIN or adenocarcinoma than in TG prostates presenting less advanced changes or normal epithelium (Figure 3*B*).

Stromal hyperplasia, inflammation, mucinous metaplasia, and epithelial hyperplasia were found to be factors with significant predictive ability for mPIN lesions by LRAs, and the predictive ability of these factors remained significant when age-adjusted analyses were performed (Table W2). Age was also found to be significantly associated with mPIN lesions by LRA ($P = .0051$; odds ratio, 1.20; 95% confidence interval, 1.06-1.37).

FGF-8b TG Prostates Present Epithelial Dedifferentiation and Collagen-Rich Stroma

In most cases, epithelial cells in mPIN lesions of TG mice showed positive staining for cytokeratins. However, areas of decreased staining for cytokeratins were found in some mPIN lesions and especially in adenocarcinoma and carcinosarcoma lesions indicating dedifferentiation of transformed epithelial cells (Figure 4*A*). Atypical stromal cells and sarcoma-like lesions in TG prostates were negative for cytokeratins.

Laminin staining, visualizing the basal lamina, was often more pronounced in TG prostates presenting stromal hypercellularity than in WT prostates, and a thickened laminin-positive layer was observed around the glands (Figure 4*A*). In contrast, a discontinuous layer of laminin-positive cells around the epithelial structures was frequently observed in TG prostates containing mPIN, carcinoma, or sarcoma-like lesions. Disruption of laminin-positive layer was most obvious in prostates containing malignant changes.

Immunostaining for smooth muscle α-actin (SMA) showed that in histologically normal WT and TG prostates, most stromal cells were positive for SMA and formed a circular layer surrounding the acini (Figure 4*A*). In contrast, in TG prostates with stromal hypercellularity, the periacinar stromal cells were negative for SMA. Similarly, the atypical stroma surrounding mPIN lesions and adenocarcinomas was SMA-negative, and sarcomatoid foci were almost completely negative for SMA.

Masson trichrome staining was performed to further characterize the hypercellular stroma in TG prostates (Figure 4*A*). Prostates from young and old TG mice containing stromal proliferation and relatively normal epithelium or early PIN lesions showed increased blue green staining around the glandular structures, indicating the presence of increased amount of collagen fibers, which are mainly produced by fibroblastic cells. Atypical stroma around more advanced mPIN lesions and adenocarcinoma and in sarcoma-like foci showed mixed, disorganized staining patterns of purple and blue green.

FGF-8b Expression Induces Formation of Collagen-Rich Periacinar Stroma in Prepubertal TG Mice

To further study the effect of FGF-8b, expression of the androgen-driven ARR_2PB-FGF-8b transgene was induced by treating prepubertal (14-day-old) mice with testosterone for a 2-week period. The induction of transgene expression by the treatment in TG prostates was verified by FGF-8 IHC (data not shown). The epithelial morphology in the prostates of androgen-treated TG animals did not differ from that of WT mice, but a slightly thickened layer of periacinar stroma was observed in VPs of TG mice. This newly formed stroma stained blue green in Masson trichrome staining (Figure 4*B*), indicating that it was rich in collagen, in a manner similar to the hypercellular stroma seen in the prostates of adult (3- to 6-month-old) TG mice.

Expression of SPP1 and CTGF Is Upregulated in FGF-8b TG Mouse Prostates

To study potential differences in gene expression between TG and WT mice, VP samples of 3-month-old TG and WT mice were analyzed using Illumina Sentrix Mouse-6 oligomicroarray BeadChips. On the basis of the results of the microarray analysis (data not shown), 13 genes (Table 1) that showed differential expression between TG and WT mice were selected for validation by qRT-PCR. The results confirmed that the expression levels of *SPP1*, *CTGF*, apolipoprotein D (*APOD*), and forkhead box 1 (*FOXQ1*) were significantly upregulated in young TG mice compared with those in WT mice (*t* and Mann-Whitney *U* tests, $P = .028$, $P = .004$, $P = .009$, and $P = .047$, respectively). A tendency toward higher expression levels of early growth response 1 (*EGR1*) in 3-month-old TG mice was also verified (*t* test, $P = .067$). For *SPP1* and *CTGF*, a significantly upregulated expression was also verified in older (12- and 15-month-old) TG mice (Figure 5*A*). Immunohistochemical stainings demonstrated that in TG prostates with stromal proliferation, stromal cells, especially adjacent to the epithelium, were positive for SPP1 (Figure 5*B*). In mPIN and adenocarcinoma lesions, some of the epithelial cells also showed positive immunostaining for SPP1.

FGF-8 TG Mouse Prostates Display Altered AR Expression

Immunohistochemical staining of AR was carefully evaluated by estimating the occurrence of AR-positive cells in prostate epithelium and stroma of TG and WT mice. Similar to WT mice, almost all nuclei were positive for AR in the normal epithelium of young TG mice (Figure 6, *A*, *a* and *b*, and *B*). In mPIN foci and adenocarcinoma lesions, the staining pattern of AR was more heterogeneous, and in many cases, the percentage of AR-positive cells was clearly decreased (Figure 6, *A*, *c* and *d* and *B*). In normal or hyperplastic stroma of TG mice, the frequency of AR-positive cells was also lower than that in the stroma of WT mice (Figure 6, *A*, *a* and *c*, and *B*). In contrast to this, the frequency of AR-positive cells was high in stromal areas containing atypical hyperplasia and especially in sarcoma-like foci (Figure 6, *A*, *e* and *f*, and *B*).

Discussion

Increased expression of FGF-8 has been reported in human premalignant PIN lesions and prostate cancer [9–11], and it has been shown to correlate with advanced stage and grade of the prostate malignancy [12,20]. To study the mechanisms by which FGF-8b affects the prostate, we generated a transgenic mouse model with a prostate targeted overexpression of FGF-8b, which was, based on previous results of Song et al. [4], expected to lead to mPIN lesion formation. Our results demonstrate that FGF-8b expression induced development of mPIN lesions,

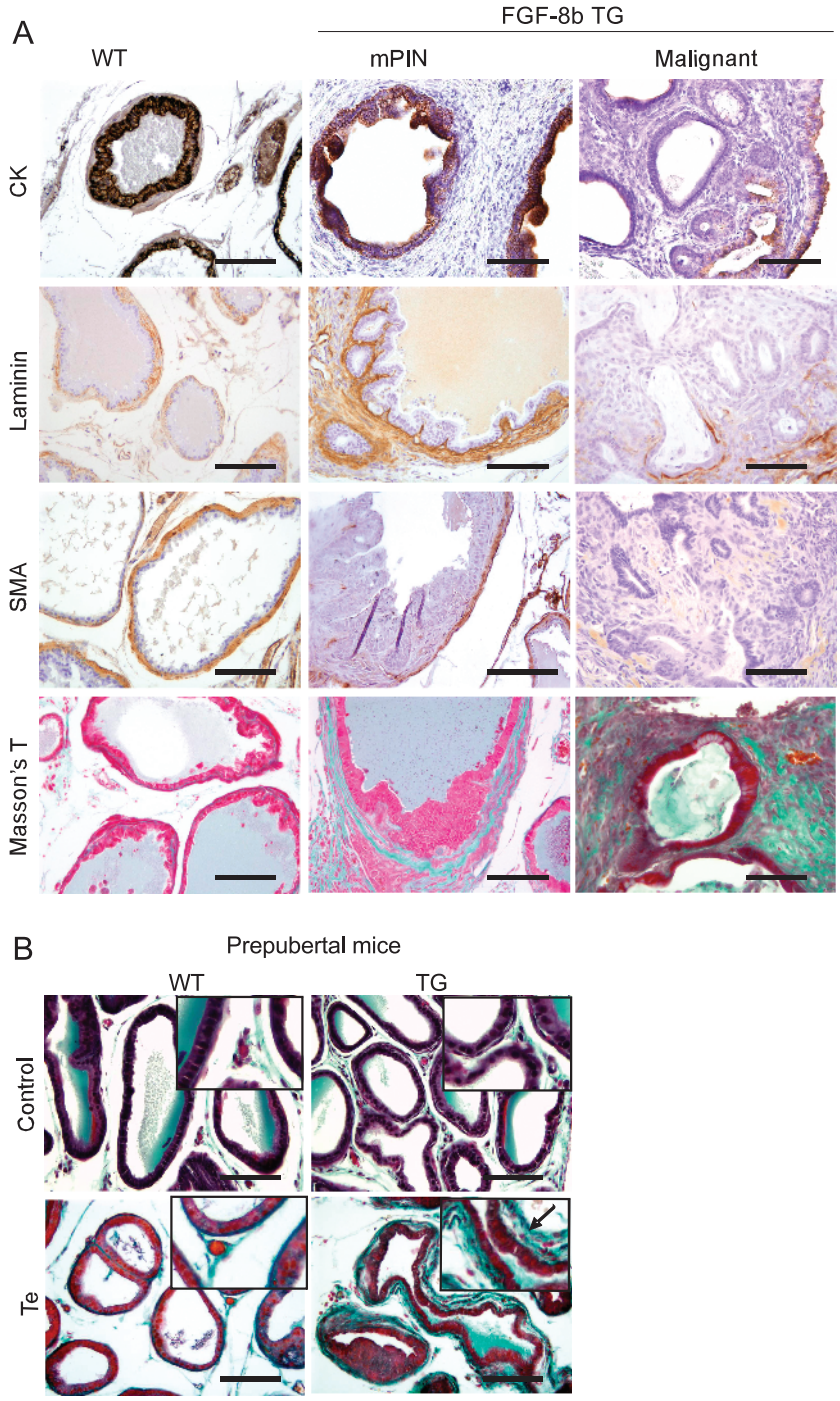

Figure 4. Altered staining for cytokeratins, laminin, and smooth muscle actin in FGF-8b TG mouse prostates. (A) Immunohistochemical staining for cytokeratins (CKs), laminin, smooth muscle α-actin (SMA), and Masson trichrome staining. VP samples from WT mice (left panel), TG mice with mPIN and stromal hypercellularity (middle panel), and a TG mouse with carcinosarcoma (right panel). Magnification, ×200. Scale bar, 100 μm. (B) Masson trichrome staining of VP sections of prepubertal (28-day-old) WT and TG mice. A thicker layer of blue green–stained stroma (arrow) was detected around the acini of TG mice administrated 14 days with testosterone-propionate (Te) than around those of the WT mice with the corresponding treatment (lower panel). Control mice (upper panel) were treated in the similar manner without testosterone. Magnification, ×200. Inserts, ×400. Scale bars, 100 μm.

which was preceded by and associated with strong stromal stimulation. Our study also shows for the first time that, except for the development of mPIN lesions [4], prolonged overexpression of FGF-8b in mouse prostate leads to prostate cancer with mixed histologic features of adenocarcinoma and sarcoma.

Our results suggest that stromal activation is an early event preceding and possibly facilitating the development of mPIN lesions in the prostates of FGF-8b TG mice. Signs of stromal stimulation and accumulation of collagen-rich stroma were observed around normal prostatic acini of young adult TG mice (3- to 6-month-old). Stromal proliferation

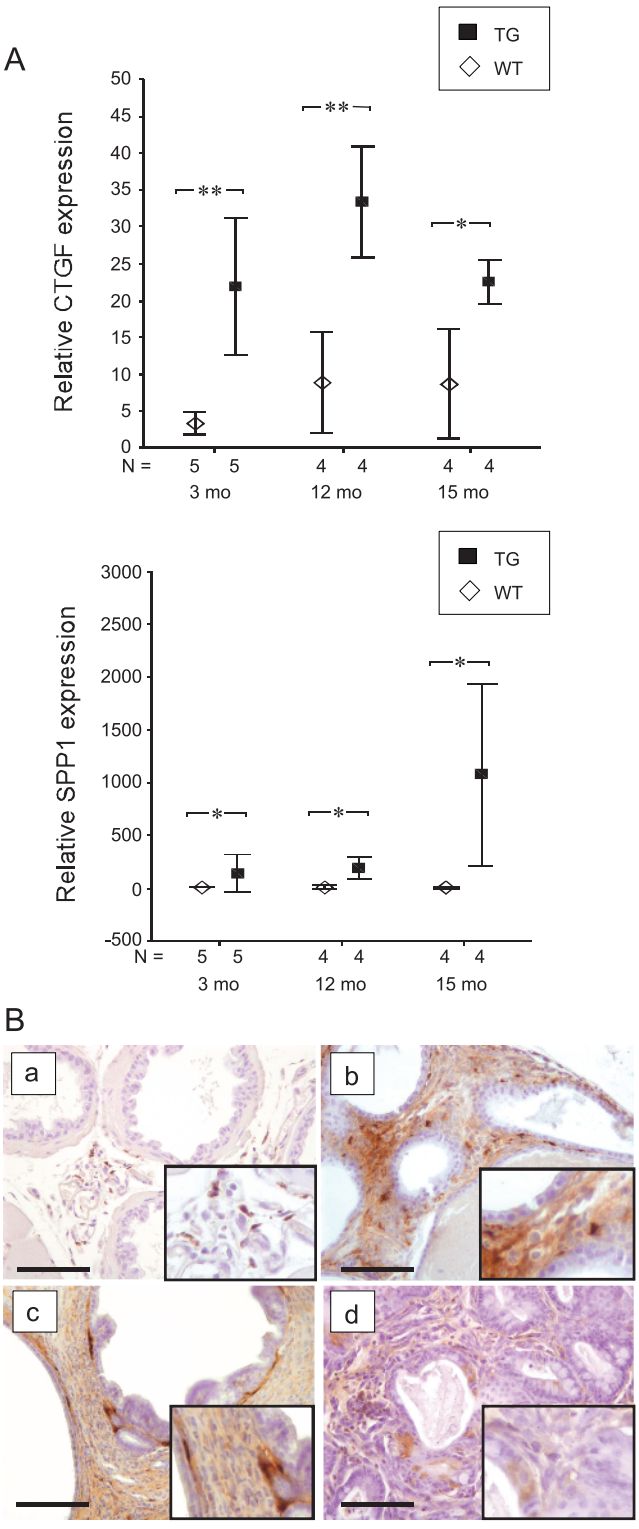

Figure 5. Up-regulation of *CTGF* and *SPP1* expression in TG mouse prostates. (A) qRT-PCR analysis of relative expression levels of *CTGF* and *SPP1* mRNA in FGF-8b–TG and WT mouse VPs in three age groups. The lowest expression value among WT mouse samples was used as a reference and set to 1. Statistical significance was assessed with the *t* test (*CTGF*) or the Mann-Whitney *U* tests (*SPP1*). $^{**}P < .01$, $^{*}P < .05$. (B) Immunohistochemical staining of SPP1 in WT mouse VP (a), in TG mouse VP with stromal proliferation (b), in TG mouse VP with mPIN (c), and in TG mouse prostate with carcinosarcoma (d). Magnification, ×200. Inserts, ×400. Scale bars, 100 μm.

could also be induced by a short (2-week) testosterone treatment of prepubertal (14-day-old) TG mice, which further suggests that it was an increased expression of the androgen-driven FGF-8b transgene that led to stromal stimulation before the appearance of epithelial changes. Primary stromal responses could be expected because the FGFR c-isoforms binding the epithelium-secreted FGF-8b are known to be more abundant in the stromal than in the epithelial compartment [2]. Our results differ from those of the earlier FGF-8 TG study [4], which reported development of histologic changes primarily in the prostate epithelium, whereas the stromal changes appeared late, generally in mice older than 17 months.

The expanded prostate stroma of TG mice showed increased histochemical staining for collagen fibers, whereas immunostaining for SMA was gradually lost on tumorigenesis, suggesting that the hypercellular changes were mainly formed by fibroblastic cells. Inflammation and increased vasculature were also seen in hypercellular prostatic stroma of our TG mice. Advanced stromal alterations and inflammation were found to be associated with epithelial changes in the prostates of our FGF-8b TG mice. Accordingly, stromal hypercellularity and inflammation were found to be predictive for the presence of mPIN lesions. These results support the idea that stromal activation facilitated the development of mPIN lesions and carcinoma in TG mouse prostates. Stromal hypercellularity and inflammation observed in our TG mice resemble characteristics of the "reactive stroma" found in association with human PIN lesions and prostate cancer [31]. Previous studies with xenograft models in which LNCaP prostate cancer cells were grown together with human prostate stromal cells in nude mice have demonstrated that reactive stroma can promote prostate tumorigenesis for example by inducing angiogenesis [32]. Reactive stroma has also been shown to be a marker for human cancer progression [33].

In the microarray analysis of the gene expression patterns in FGF-8b TG and WT mouse VPs, *SPP1* and *CTGF* were identified as highly upregulated genes in TG mice. The qRT-PCR validation analyses confirmed the results and showed that these genes were strongly upregulated in the prostates of both young and old FGF-8b TG mice. Previous studies have associated CTGF and SPP1 with the development of activated stroma and inflammation [34,35], which suggests that these genes play an important role in the prostate alterations of our FGF-8b TG mice. Increased expression of SPP1 has been linked to prostate tumorigenesis and metastasis in several studies [36,37], and there is evidence, that in experimental prostate cancer models, its expression is induced by FGF-8 [25,38] and by activation of FGFR1 [39]. In contrast to previous studies that have reported an increased expression of SPP1 by the transformed epithelium [38], our present data suggest that, in the FGF-8b TG mouse prostates, SPP1 is primarily produced by the hypercellular stroma and only to a limited extent by transformed epithelial cells. Stromal origin of SPP1 is in line with the results from our previous study [25], which showed that expression of *SPP1* was upregulated in FGF-8b–overexpressing orthotopic PC-3 tumors but not in *in vitro* cultures of FGF-8b–transfected PC-3 cells. It is possible that stromal SPP1 functions as an important preneoplastic cell growth–promoting factor as suggested by Pazolli et al. [40]. Up-regulation of another gene, *APOD*, observed in TG prostates in our microarray study could also be linked to increased SPP1 [41]. *APOD* has been shown to be a marker of high-grade PIN and prostate cancer in humans [42] but its function in the prostate is unknown. Increased expression of *CTGF* in FGF-8 TG prostates is also in line with the phenotype of activated stroma because CTGF has been shown to be a mediator of TGF-β induced formation of reactive stroma, angiogenesis

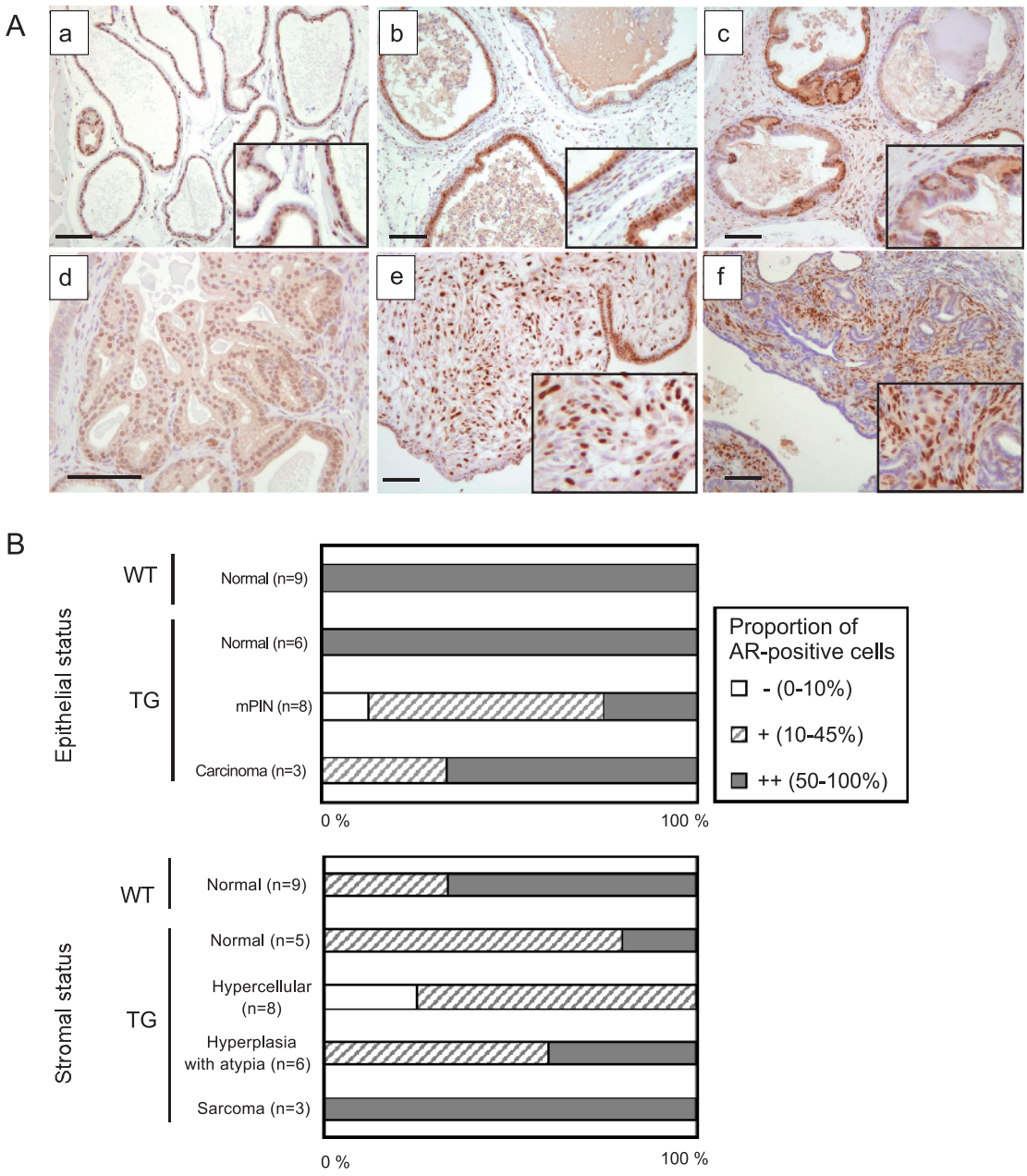

Figure 6. FGF-8b TG mouse prostates present altered AR staining. (A) IHC staining of AR in VP of a WT mouse (a), in TG prostate with stromal hypercellularity and inflammation (b), in an mPIN focus of a TG mouse (c), in adenocarcinoma (d), in sarcoma (e), and in carcinosarcoma (f). Magnification: all, ×100; d, ×200. Inserts, ×200. Scale bars, 100 μm. (B) Staining grades in AR IHC in VP epithelium (upper graph) and stroma (lower graph) of WT and TG mice with normal and altered histology. Grades were evaluated as proportion of AR-positive cells in the VP areas with respective changes as indicated in the Materials and Methods section.

and tumor growth [35]. Our previous studies have demonstrated that FGF-8 increases angiogenesis [22,24], and rich vasculature was also seen in the hypercellular stroma of TG mice. Up-regulation of *CTGF* could be one of the mechanisms mediating this effect of FGF-8.

The malignancies in the prostate of old FGF-8b TG mice displayed a highly variable morphology including adenocarcinoma, sarcoma, and carcinosarcoma-like lesions. It is intriguing that the mixed neoplastic lesions in the FGF-8b TG mouse prostates showed marked similarities to those observed in the FGFR1 TG mice [8], in which FGF pathways had been disrupted by inducing FGFR1 activation in the prostate epithelium. This suggests that FGFR1 is involved in the induction of malignant development in the FGF-8b TG prostates and that the mechanisms underlying the development of mixed prostate tumor phenotype in two mouse models could also bear similarities. However, activation of other FGF-8b binding FGFRs (FGFR2c, -3c, and -4) expressed in prostate [2] is also possible in the FGF-8b TG mice. Induction of *FGFR2c* expression has been reported in transformed prostate epithelium [43,44], but previous studies have shown that the transgenic mice expressing activated FGFR2c in epithelium do not develop hyperplasias or dysplasias like those with the activated FGFR1c [6]. There is also evidence that epithelial FGFR2 is required to maintain normal tissue homeostasis in prostate and could have a role opposite that of FGFR1 in prostate tumorigenesis [45]. There is less information on the role of FGFR2c in prostate stroma, but in

FGF-8b–expressing TG prostates, it might contribute to stromal activation. FGFR3 does not seem to have a central role in the pathogenesis of prostate cancer [44,46], whereas increased epithelial expression and a polymorphism of the *FGFR4* gene have been associated with human prostate cancer progression [44,47]. Taken together, altered function of different FGFRs in epithelium and stroma can contribute to the observed prostate phenotypes in FGF-8b TG mice in a complex way.

The heterogeneous tumor phenotype in the FGF-8b TG prostates raises the question of which cell type(s), particularly in the case of sarcoma-like foci, have given origin to tumor cells. In the FGFR1 TG model formation of "sarcomatoid carcinomas" was suggested to result from an epithelial-to-mesenchymal transition (EMT) and subsequent invasion of epithelium-derived tumor cells to stroma [8,48]. We have previously found that FGF-8b induces fibroblastic phenotype and anchorage independent growth in S115 breast cancer cells [22], which supports a possibility of EMT in appearance of malignant cells in prostatic stroma of our FGF-8b TG mice. In addition, stromal tumor cells in our FGF-8b TG mice expressed AR, which also speaks for the possibility of transdifferentiation of epithelium-derived tumor cells to sarcoma-like phenotype. The decreased cytokeratin staining in the transformed epithelial cells of adenocarcinoma and carcinosarcoma lesions could also be interpreted as a sign of EMT. Nevertheless, positive immunostaining of FGF-8b in the adenocarcinomas and negative staining in the sarcomas and carcinosarcomas could be interpreted as a sign of different origin of these lesions, which suggests that the stromal malignancies are formed by secondary mechanisms. With the present data, it is, however, impossible to determine the cellular origin of sarcoma-like lesions in the FGF-8b TG mice.

The expression of AR was decreased in normal and hypercellular stroma as well as in dysplastic and malignant epithelium of TG prostates. The decrease of stromal AR is in line with our other results indicating increased proportion of fibroblastic and decreased smooth muscle cells in TG prostates because AR is known to be expressed by smooth muscle cells in the normal prostate stroma, whereas most fibroblastic cells are negative for AR [49]. The decrease in epithelial AR expression could be associated with epithelial dedifferentiation. Stromal ARs are considered to regulate normal differentiation and function of prostatic epithelium and to repress epithelial proliferation [50]. Accordingly, Wikstrom et al. [51] recently reported that lowered AR in prostate stroma is related to poor prognosis in prostate cancer patients. Therefore, decrease of AR in the hypercellular but nontransformed stroma of our TG mice could be one of the mechanisms behind increased epithelial proliferation and dedifferentiation.

Opposite the normal and hypercellular TG prostate, stroma AR-positive cells were abundant in atypical stroma and especially in the areas of carcinosarcoma and sarcoma-like lesions. These AR-positive cells were SMA-negative, which suggests fibroblastic or epithelial origin. It is possible, as discussed earlier, that these AR-positive cells are epithelium-derived stroma-invaded cells as suggested for FGFR1 TG prostates [8]. Another possibility is that AR expression is upregulated in malignant stromal cells of TG prostates. Some of the lesions in FGF-8b TG prostates resemble "stromal tumors of uncertain malignant potential" (STUMPs), which are rare stromal lesions in human prostate [52]. Most of the human STUMPs are benign, but a subset can develop to sarcomas. The phyllodes growth pattern seen in a subset of human STUMPs and sarcomas was also seen in stromal atypias of FGF-8b TG mice. Interestingly, strong AR expression has been reported for human STUMPs and sarcomas [53]. Taken together, alterations in the AR expression in FGF-8b TG mouse prostates suggest that autocrine/paracrine FGF signaling can directly or indirectly modulate AR levels as has been shown for other growth factor pathways [54]. In line with this, increased stromal FGF-10 has been shown to enhance

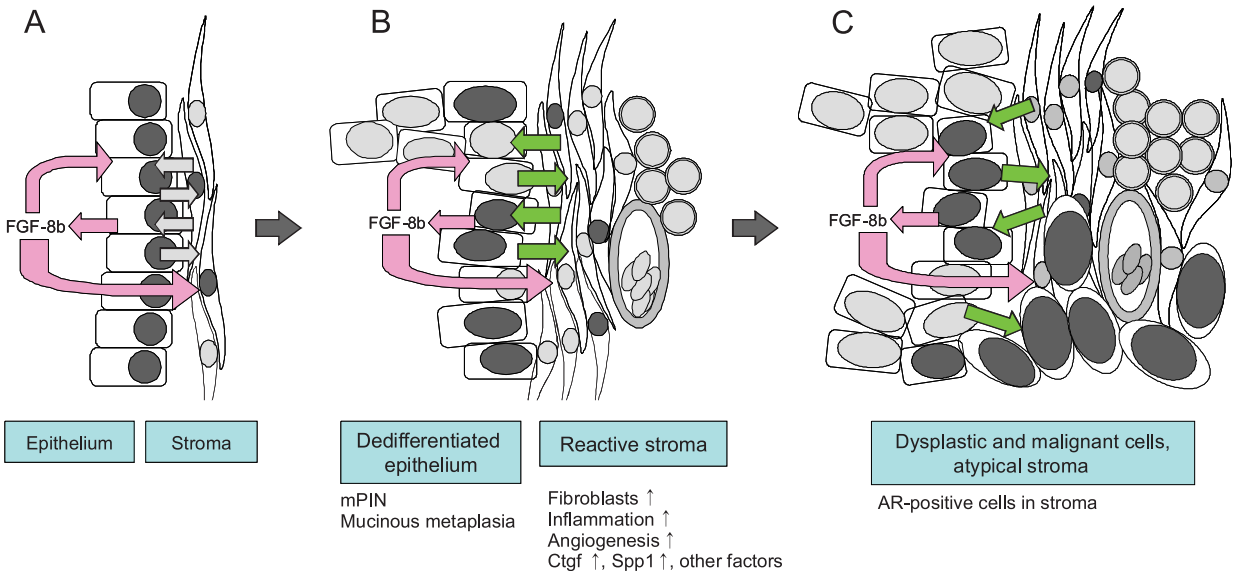

Figure 7. A proposed model for FGF-8 action in prostate. (A) Increased levels of FGF-8b are secreted by the epithelial cells. It affects both the epithelium and the stroma (autocrine and paracrine effects, pink arrows). (B) The affected stroma presents features of reactive stroma, such as increased amount of fibroblasts, inflammation, and angiogenesis. Altered stroma secretes connective tissue growth factor (*CTGF*), *SPP1*, and other (unidentified) factors that can affect the epithelium. The disturbed cross talk (indicated by green arrows) between stromal and epithelial compartment together with increased amounts of FGF-8b induce proliferation and dedifferentiation of the epithelium, leading to the development of preneoplastic mPIN lesions. (C) Prolonged FGF-8b exposure and disturbed epithelial-to-stromal cross talk induces the epithelium and the stroma to develop atypical and malignant changes. AR-positive nuclei are presented by dark gray; AR-negative nuclei, light gray color.

the level of epithelial AR in tissue recombination experiments in which FGF-10–expressing urogenital sinus mesenchyme cells and prostate epithelial cells were grafted under the mouse kidney capsule [55].

In conclusion, our study provides evidence that FGF-8b is able to induce development of mPIN lesions and very heterogeneous prostate cancer with features of adenocarcinoma, carcinosarcoma, and sarcoma in the mouse. Development of PIN lesions and other neoplastic changes were preceded by and associated with the activation of stroma. We propose that besides an autocrine effect on the epithelium, paracrine activation of the stroma leading to disrupted cross talk between epithelium and stroma is an equally important factor in FGF-8b–induced prostate tumorigenesis (Figure 7). The results suggest that FGF-8 commonly expressed at an increased level in human PIN lesions and tumor tissue contributes to development and progression of prostate cancer via paracrine activation of stroma.

Acknowledgments

The authors thank S. Jussila, L. Shumskaya, S. Auer, L. Simola and L. Jacobsson for excellent technical assistance. R.J. Matusik (Vanderbilt University Medical Center, Nashville, TN) is acknowledged for providing the ARR_2PB promoter construct, P. Roy-Burman (University of California – Los Angeles, California) for providing the human FGF-8b cDNA expression vector. Biostatistician S. Hurme and Dr. K. Ivaska are acknowledged for assistance with the statistical tests.

References

[1] Beenken A and Mohammadi M (2009). The FGF family: biology, pathophysiology and therapy. *Nat Rev Drug Discov* **8**, 235–253.

[2] Kwabi-Addo B, Ozen M, and Ittmann M (2004). The role of fibroblast growth factors and their receptors in prostate cancer. *Endocr Relat Cancer* **11**, 709–724.

[3] Li ZG, Mathew P, Yang J, Starbuck MW, Zurita AJ, Liu J, Sikes C, Multani AS, Efstathiou E, Lopez A, et al. (2008). Androgen receptor–negative human prostate cancer cells induce osteogenesis in mice through FGF9-mediated mechanisms. *J Clin Invest* **118**, 2697–2710.

[4] Song Z, Wu X, Powell WC, Cardiff RD, Cohen MB, Tin RT, Matusik RJ, Miller GJ, and Roy-Burman P (2002). Fibroblast growth factor 8 isoform B overexpression in prostate epithelium: a new mouse model for prostatic intraepithelial neoplasia. *Cancer Res* **62**, 5096–5105.

[5] Chua SS, Ma ZQ, Gong L, Lin SH, DeMayo FJ, and Tsai SY (2002). Ectopic expression of FGF-3 results in abnormal prostate and wolffian duct development. *Oncogene* **21**, 1899–1908.

[6] Freeman KW, Welm BE, Gangula RD, Rosen JM, Ittmann M, Greenberg NM, and Spencer DM (2003). Inducible prostate intraepithelial neoplasia with reversible hyperplasia in conditional FGFR1-expressing mice. *Cancer Res* **63**, 8256–8263.

[7] Wang F, McKeehan K, Yu C, Ittmann M, and McKeehan WL (2004). Chronic activity of ectopic type 1 fibroblast growth factor receptor tyrosine kinase in prostate epithelium results in hyperplasia accompanied by intraepithelial neoplasia. *Prostate* **58**, 1–12.

[8] Acevedo VD, Gangula RD, Freeman KW, Li R, Zhang Y, Wang F, Ayala GE, Peterson LE, Ittmann M, and Spencer DM (2007). Inducible FGFR-1 activation leads to irreversible prostate adenocarcinoma and an epithelial-to-mesenchymal transition. *Cancer Cell* **12**, 559–571.

[9] Tanaka A, Furuya A, Yamasaki M, Hanai N, Kuriki K, Kamiakito T, Kobayashi Y, Yoshida H, Koike M, and Fukayama M (1998). High frequency of fibroblast growth factor (FGF) 8 expression in clinical prostate cancers and breast tissues, immunohistochemically demonstrated by a newly established neutralizing monoclonal antibody against FGF 8. *Cancer Res* **58**, 2053–2056.

[10] Leung HY, Dickson C, Robson CN, and Neal DE (1996). Over-expression of fibroblast growth factor-8 in human prostate cancer. *Oncogene* **12**, 1833–1835.

[11] Valve EM, Nevalainen MT, Nurmi MJ, Laato MK, Martikainen PM, and Harkonen PL (2001). Increased expression of FGF-8 isoforms and FGF receptors in human premalignant prostatic intraepithelial neoplasia lesions and prostate cancer. *Lab Invest* **81**, 815–826.

[12] Gnanapragasam VJ, Robinson MC, Marsh C, Robson CN, Hamdy FC, and Leung HY (2003). FGF8 isoform b expression in human prostate cancer. *Br J Cancer* **88**, 1432–1438.

[13] Marsh SK, Bansal GS, Zammit C, Barnard R, Coope R, Roberts-Clarke D, Gomm JJ, Coombes RC, and Johnston CL (1999). Increased expression of fibroblast growth factor 8 in human breast cancer. *Oncogene* **18**, 1053–1060.

[14] Valve E, Martikainen P, Seppanen J, Oksjoki S, Hinkka S, Anttila L, Grenman S, Klemi P, and Harkonen P (2000). Expression of fibroblast growth factor (FGF)-8 isoforms and FGF receptors in human ovarian tumors. *Int J Cancer* **88**, 718–725.

[15] Ohuchi H, Yoshioka H, Tanaka A, Kawakami Y, Nohno T, and Noji S (1994). Involvement of androgen-induced growth factor (FGF-8) gene in mouse embryogenesis and morphogenesis. *Biochem Biophys Res Commun* **204**, 882–888.

[16] MacArthur CA, Lawshe A, Xu J, Santos-Ocampo S, Heikinheimo M, Chellaiah AT, and Ornitz DM (1995). FGF-8 isoforms activate receptor splice forms that are expressed in mesenchymal regions of mouse development. *Development* **121**, 3603–3613.

[17] Zhang X, Ibrahimi OA, Olsen SK, Umemori H, Mohammadi M, and Ornitz DM (2006). Receptor specificity of the fibroblast growth factor family. The complete mammalian FGF family. *J Biol Chem* **281**, 15694–15700.

[18] Gemel J, Gorry M, Ehrlich GD, and MacArthur CA (1996). Structure and sequence of human FGF8. *Genomics* **35**, 253–257.

[19] MacArthur CA, Lawshe A, Shankar DB, Heikinheimo M, and Shackleford GM (1995). FGF-8 isoforms differ in NIH3T3 cell transforming potential. *Cell Growth Differ* **6**, 817–825.

[20] Murphy T, Darby S, Mathers ME, and Gnanapragasam VJ (2010). Evidence for distinct alterations in the FGF axis in prostate cancer progression to an aggressive clinical phenotype. *J Pathol* **4**, 452–460.

[21] Dorkin TJ, Robinson MC, Marsh C, Bjartell A, Neal DE, and Leung HY (1999). FGF8 over-expression in prostate cancer is associated with decreased patient survival and persists in androgen independent disease. *Oncogene* **18**, 2755–2761.

[22] Mattila MM, Ruohola JK, Valve EM, Tasanen MJ, Seppanen JA, and Harkonen PL (2001). FGF-8b increases angiogenic capacity and tumor growth of androgen-regulated S115 breast cancer cells. *Oncogene* **20**, 2791–2804.

[23] Ruohola JK, Viitanen TP, Valve EM, Seppanen JA, Loponen NT, Keskitalo JJ, Lakkakorpi PT, and Harkonen PL (2001). Enhanced invasion and tumor growth of fibroblast growth factor 8b–overexpressing MCF-7 human breast cancer cells. *Cancer Res* **61**, 4229–4237.

[24] Valta MP, Tuomela J, Bjartell A, Valve E, Vaananen HK, and Harkonen P (2008). FGF-8 is involved in bone metastasis of prostate cancer. *Int J Cancer* **123**, 22–31.

[25] Valta MP, Tuomela J, Vuorikoski H, Loponen N, Vaananen RM, Pettersson K, Vaananen HK, and Harkonen PL (2009). FGF-8b induces growth and rich vascularization in an orthotopic PC-3 model of prostate cancer. *J Cell Biochem* **107**, 769–784.

[26] Zhang J, Thomas TZ, Kasper S, and Matusik RJ (2000). A small composite probasin promoter confers high levels of prostate-specific gene expression through regulation by androgens and glucocorticoids *in vitro* and *in vivo*. *Endocrinology* **141**, 4698–4710.

[27] Kallio A, Guo T, Lamminen E, Seppanen J, Kangas L, Vaananen HK, and Harkonen P (2008). Estrogen and the selective estrogen receptor modulator (SERM) protection against cell death in estrogen receptor alpha and beta expressing U2OS cells. *Mol Cell Endocrinol* **289**, 38–48.

[28] Livak KJ and Schmittgen TD (2001). Analysis of relative gene expression data using real-time quantitative PCR and the 2(–Delta Delta *C*(T)) method. *Methods* **25**, 402–408.

[29] Jiborn T, Abrahamson M, Wallin H, Malm J, Lundwall A, Gadaleanu V, Abrahamsson PA, and Bjartell A (2004). Cystatin C is highly expressed in the human male reproductive system. *J Androl* **25**, 564–572.

[30] Shappell SB, Thomas GV, Roberts RL, Herbert R, Ittmann MM, Rubin MA, Humphrey PA, Sundberg JP, Rozengurt N, Barrios R, et al. (2004). Prostate pathology of genetically engineered mice: definitions and classification. The consensus report from the Bar Harbor Meeting of the Mouse Models of Human Cancer Consortium Prostate Pathology Committee. *Cancer Res* **64**, 2270–2305.

[31] Tuxhorn JA, Ayala GE, Smith MJ, Smith VC, Dang TD, and Rowley DR (2002). Reactive stroma in human prostate cancer: induction of myofibroblast phenotype and extracellular matrix remodeling. *Clin Cancer Res* **8**, 2912–2923.

[32] Tuxhorn JA, McAlhany SJ, Dang TD, Ayala GE, and Rowley DR (2002). Stromal cells promote angiogenesis and growth of human prostate tumors in a differential reactive stroma (DRS) xenograft model. *Cancer Res* **62**, 3298–3307.

[33] Ayala G, Tuxhorn JA, Wheeler TM, Frolov A, Scardino PT, Ohori M, Wheeler M, Spitler J, and Rowley DR (2003). Reactive stroma as a predictor of biochemical-free recurrence in prostate cancer. *Clin Cancer Res* **9**, 4792–4801.

[34] Wang KX and Denhardt DT (2008). Osteopontin: role in immune regulation and stress responses. *Cytokine Growth Factor Rev* **19**, 333–345.

[35] Yang F, Tuxhorn JA, Ressler SJ, McAlhany SJ, Dang TD, and Rowley DR (2005). Stromal expression of connective tissue growth factor promotes angiogenesis and prostate cancer tumorigenesis. *Cancer Res* **65**, 8887–8895.

[36] Castellano G, Malaponte G, Mazzarino MC, Figini M, Marchese F, Gangemi P, Travali S, Stivala F, Canevari S, and Libra M (2008). Activation of the osteopontin/matrix metalloproteinase-9 pathway correlates with prostate cancer progression. *Clin Cancer Res* **14**, 7470–7480.

[37] Ramankulov A, Lein M, Kristiansen G, Loening SA, and Jung K (2007). Plasma osteopontin in comparison with bone markers as indicator of bone metastasis and survival outcome in patients with prostate cancer. *Prostate* **67**, 330–340.

[38] Khodavirdi AC, Song Z, Yang S, Zhong C, Wang S, Wu H, Pritchard C, Nelson PS, and Roy-Burman P (2006). Increased expression of osteopontin contributes to the progression of prostate cancer. *Cancer Res* **66**, 883–888.

[39] Freeman KW, Gangula RD, Welm BE, Ozen M, Foster BA, Rosen JM, Ittmann M, Greenberg NM, and Spencer DM (2003). Conditional activation of fibroblast growth factor receptor (FGFR) 1, but not FGFR2, in prostate cancer cells leads to increased osteopontin induction, extracellular signal–regulated kinase activation, and *in vivo* proliferation. *Cancer Res* **63**, 6237–6243.

[40] Pazolli E, Luo X, Brehm S, Carbery K, Chung JJ, Prior JL, Doherty J, Demehri S, Salavaggione L, Piwnica-Worms D, et al. (2009). Senescent stromal-derived osteopontin promotes preneoplastic cell growth. *Cancer Res* **69**, 1230–1239.

[41] Jin D, El-Tanani M, and Campbell FC (2006). Identification of apolipoprotein D as a novel inhibitor of osteopontin-induced neoplastic transformation. *Int J Oncol* **29**, 1591–1599.

[42] Hall RE, Horsfall DJ, Stahl J, Vivekanandan S, Ricciardelli C, Stapleton AM, Scardino PT, Neufing P, and Tilley WD (2004). Apolipoprotein-D: a novel cellular marker for HGPIN and prostate cancer. *Prostate* **58**, 103–108.

[43] Yan G, Fukabori Y, McBride G, Nikolaropolous S, and McKeehan WL (1993). Exon switching and activation of stromal and embryonic fibroblast growth factor (FGF)–FGF receptor genes in prostate epithelial cells accompany stromal independence and malignancy. *Mol Cell Biol* **13**, 4513–4522.

[44] Sahadevan K, Darby S, Leung HY, Mathers ME, Robson CN, and Gnanapragasam VJ (2007). Selective over-expression of fibroblast growth factor receptors 1 and 4 in clinical prostate cancer. *J Pathol* **213**, 82–90.

[45] Jin C, McKeehan K, Guo W, Jauma S, Ittmann MM, Foster B, Greenberg NM, McKeehan WL, and Wang F (2003). Cooperation between ectopic FGFR1 and depression of FGFR2 in induction of prostatic intraepithelial neoplasia in the mouse prostate. *Cancer Res* **63**, 8784–8790.

[46] Gowardhan B, Douglas DA, Mathers ME, McKie AB, McCracken SR, Robson CN, and Leung HY (2005). Evaluation of the fibroblast growth factor system as a potential target for therapy in human prostate cancer. *Br J Cancer* **92**, 320–327.

[47] Wang J, Stockton DW, and Ittmann M (2004). The fibroblast growth factor receptor-4 Arg388 allele is associated with prostate cancer initiation and progression. *Clin Cancer Res* **10**, 6169–6178.

[48] Thiery JP (2002). Epithelial-mesenchymal transitions in tumour progression. *Nat Rev Cancer* **2**, 442–454.

[49] Prins GS, Birch L, and Greene GL (1991). Androgen receptor localization in different cell types of the adult rat prostate. *Endocrinology* **129**, 3187–3199.

[50] Cunha GR, Hayward SW, Wang YZ, and Ricke WA (2003). Role of the stromal microenvironment in carcinogenesis of the prostate. *Int J Cancer* **107**, 1–10.

[51] Wikstrom P, Marusic J, Stattin P, and Bergh A (2009). Low stroma androgen receptor level in normal and tumor prostate tissue is related to poor outcome in prostate cancer patients. *Prostate* **69**, 799–809.

[52] Hansel DE, Herawi M, Montgomery E, and Epstein JI (2007). Spindle cell lesions of the adult prostate. *Mod Pathol* **20**, 148–158.

[53] Wang X, Jones TD, Zhang S, Eble JN, Bostwick DG, Qian J, Lopez-Beltran A, Montironi R, Harris JJ, and Cheng L (2007). Amplifications of *EGFR* gene and protein expression of EGFR, her-2/neu, c-kit, and androgen receptor in phyllodes tumor of the prostate. *Mod Pathol* **20**, 175–182.

[54] Zhu ML and Kyprianou N (2008). Androgen receptor and growth factor signaling cross-talk in prostate cancer cells. *Endocr Relat Cancer* **15**, 841–849.

[55] Memarzadeh S, Xin L, Mulholland DJ, Mansukhani A, Wu H, Teitell MA, and Witte ON (2007). Enhanced paracrine FGF10 expression promotes formation of multifocal prostate adenocarcinoma and an increase in epithelial androgen receptor. *Cancer Cell* **12**, 572–585.

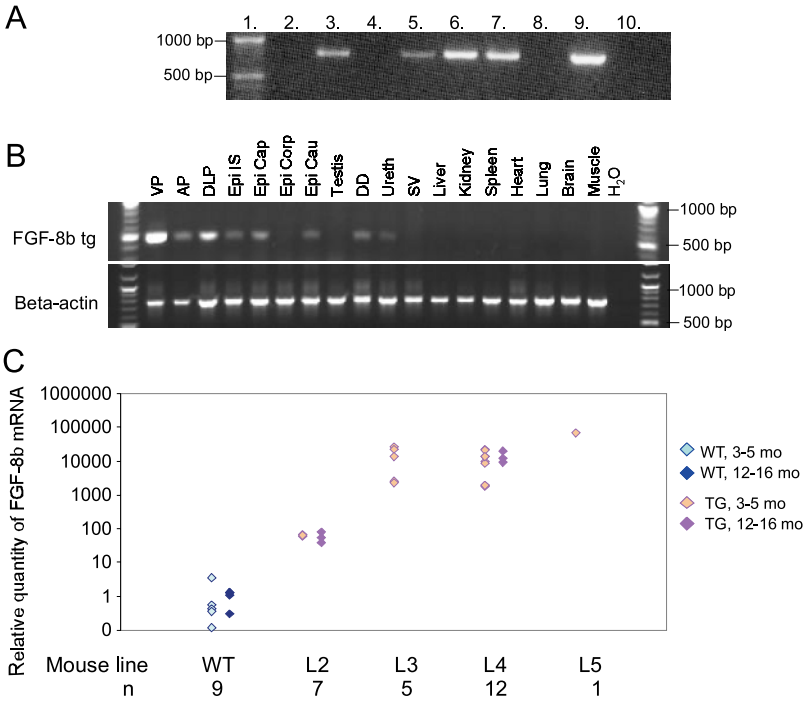

Figure W1. Generation and expression analysis of FGF-8b transgenic mice. (A) Genotyping PCR with primers specific for the transgene construct resulted in a 762-bp product from DNA samples from mice positive for the transgene (lanes 3, 5, 6, 7, and 9) and no product from WT mice (lanes 2, 4, and 8). Lane 10: negative control. (B) Analysis of *FGF-8b* expression by way of transgene-specific RT-PCR using tissues of a 3-month-old TG mouse (L4). *β-Actin* was used as an internal control for cDNA synthesis. DD indicates ductus deferens; Epi Cap, epididymis caput; Epi Cau, epididymis cauda; Epi corp, epididymis corpus; Epi IS, epididymis initial segment; SV, seminal vesicles. (C) Relative quantity of FGF-8b mRNA in VPs of WT mice and TG mice (3-5 and 12-16 months old) from different FGF-8b TG mouse lines (L2, L3, L4, and L5) studied by qRT-PCR. mo indicates months old.

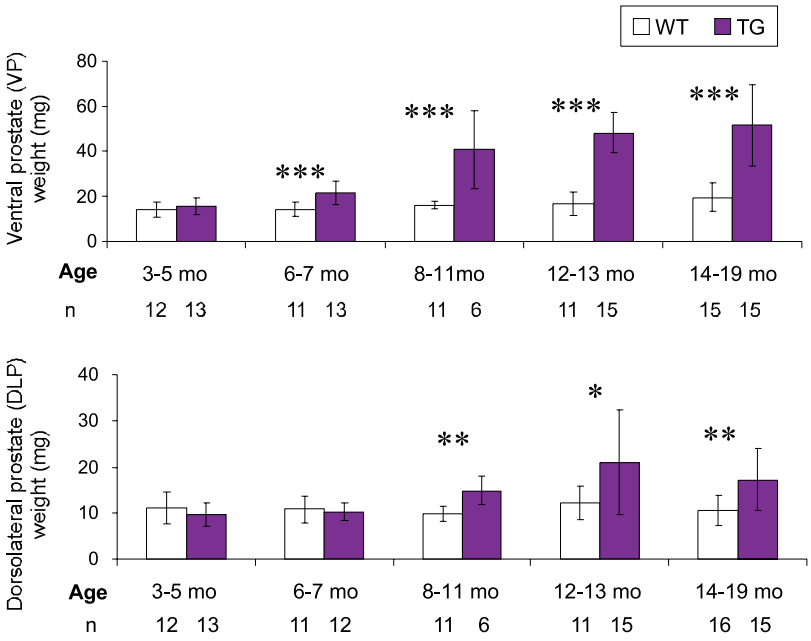

Figure W2. Weights of VP and DLP of FGF-8b–TG and WT mice in five age groups. The columns show mean ± SD. One case with a very large carcinosarcoma tumor in the VP (weight, 3871 mg) has been excluded from the oldest (14- to 19-month-old) TG group for clarity. Statistical significance was assessed with the Student's *t* test (VP) or with the Mann-Whitney *U* test (DLP). ***$P < .001$, **$P < .01$, *$P < .05$. mo indicates months old.

Table W1. Frequencies of Histologic Changes in Prostate in Three Age Groups.

	3-6 months		7-11 months		12-21 months	
	WT (*n* = 15)	TG (*n* = 18)	WT (*n* = 12)	TG (*n* = 18)	WT (*n* = 15)	TG (*n* = 32)
Dilatation of glands	—	33	—	44	7	76
Mucinous metaplasia	—	17	8	38	20	42
Epithelial hypercellularity	31	61	8	75	20	74
Epithelial hyperplasia with atypia	—	11	—	38	—	53
mPIN	—	—	—	19	—	47
Adenocarcinoma	—	—	—	—	—	8
Inflammation*	13	17	25	50	13	58
Stromal hypercellularity	19	56	0	38	7	71
Stromal hypercellularity with atypia	—	—	—	6	—	32
Sarcoma†	—	—	—	—	—	16

*Includes all degrees of inflammation (score, 0-3).
†Includes carcinosarcomas.

Table W2. Predictive Ability for mPIN Lesions of Age-Adjusted Variables Studied by Logistic Regression Analysis.

Variable	*P*	OR (CI)
Mucinous metaplasia	<.001	10.93 (2.99-39.93)
Epithelial hyperplasia	.012	11.07 (1.04-91.78)
Stromal hypercellularity	<.001	8.60 (2.50-29.60)
Inflammation	<.001	12.26 (3.02-49.84)

P values, odds ratios (OR), and 95% confidence intervals (CI) are given.